

High Relaxivity Gadolinium-Polydopamine Nanoparticles

Zhao Wang, Fabio Carniato, Yijun Xie, Yuran Huang, Yiwen Li, Sha He, Nanzhi Zang, Jeffrey D. Rinehart,* Mauro Botta,* and Nathan C. Gianneschi*

This study reports the preparation of a series of gadolinium-polydopamine nanoparticles (GdPD-NPs) with tunable metal loadings. GdPD-NPs are analyzed by nuclear magnetic relaxation dispersion and with a 7-tesla (T) magnetic resonance imaging (MRI) scanner. A relaxivity of 75 and 10.3 mM⁻¹ s⁻¹ at 1.4 and 7 T is observed, respectively. Furthermore, superconducting quantum interference device magnetometry is used to study intraparticle magnetic interactions and determine the GdPD-NPs consist of isolated metal ions even at maximum metal loadings. From these data, it is concluded that the observed high relaxivities arise from a high hydration state of the Gd(III) at the particle surface, fast rate of water exchange, and negligible antiferromagnetic coupling between Gd(III) centers throughout the particles. This study highlights design parameters and a robust synthetic approach that aid in the development of this scaffold for T₁-weighted, high relaxivity MRI contrast agents.

Contrast media are used in a third of the ≈80 million magnetic resonance imaging (MRI) exams performed worldwide each year.^[1] Those approved for clinical use are low molecular weight, paramagnetic, Gd(III) chelates. They increase the signal intensity on T₁-weighted images, shorten the examination time, improve the diagnostic confidence, and enhance the image contrast.^[2] Relaxivity, r_1 , is an important parameter that measures the ability of a Gd-complex to change R_1 ($1/T_1$) of nearby water protons. Currently used Gd-based contrast agents (CAs) exhibit only a fraction of the efficacy (r_1) predicted by theoretical models translating to a lower sensitivity

of detection than what should be attainable.^[3] This is mainly because of rapid molecular tumbling ($\tau_R < 100$ ps) and low hydration states ($q = 1$). Low r_1 values limit the use of small molecule Gd(III) chelates in targeted imaging because a large local concentration of the CAs is needed to produce a detectable change in R_1 . To overcome this limit of sensitivity, different strategies have been explored. The most common strategy involves the preparation of nanoscale or macromolecular formulations in which multiple Gd(III) chelates are associated.^[4] Since r_1 is linearly proportional to the concentration of the CA, a high payload ($\gg 100$ ions) is critical to attain a high local concentration at the biological target site; that is, for each targeting event of the macromolecule or particle species, multiple Gd(III) centers

are localized. Ideally then, these systems would possess high molecular r_1 resulting from the combined effect of the large number of Gd(III) ions and the slow global rotational motion that increases r_1 of each individual Gd-complex.^[5] Noncovalently bound MRI CAs often suffer from weak associations limiting applications in vivo. In one example, protein engineering has enabled the design of Gd-specific binding proteins that show excellent metal selectivity and stability.^[6] However, the sophisticated preparation processes prevent large-scale production with immunogenicity also being a concern. Covalently linking small molecule chelates with synthetic polymers or nanoparticles

Z. Wang, Y. Xie, Y. Huang, Dr. Y. Li, N. Zang, Prof. J. D. Rinehart, Prof. N. C. Gianneschi
Department of Chemistry and Biochemistry
University of California San Diego
La Jolla, CA 92093, USA
E-mail: jrinehart@ucsd.edu;
nathan.gianneschi@northwestern.edu

Z. Wang, Prof. N. C. Gianneschi
Department of Chemistry
Northwestern University
Evanston, IL 60208, USA

Dr. F. Carniato, Prof. M. Botta
Dipartimento di Scienze e Innovazione Tecnologica
Università del Piemonte Orientale
"A. Avogadro" Viale Teresa Michel 11
15120 Alessandria, AL, Italy
E-mail: mauro.botta@uniupo.it


Y. Xie, Y. Huang, N. Zang, Prof. J. D. Rinehart
Materials Science and Engineering
University of California
San Diego, La Jolla, CA 92093, USA

Dr. Y. Li
College of Polymer Science and Engineering
State Key Laboratory of Polymer Materials Engineering
Sichuan University
Chengdu 610065, China

Dr. S. He
Department of NanoEngineering
University of California
San Diego, La Jolla, CA 92093, USA

Prof. N. C. Gianneschi
Department of Materials Science and Engineering
Northwestern University
Evanston, IL 60208, USA

Prof. N. C. Gianneschi
Department of Biomedical Engineering
Northwestern University
Evanston, IL 60208, USA

 The ORCID identification number(s) for the author(s) of this article can be found under <https://doi.org/10.1002/sml.201701830>.

DOI: 10.1002/sml.201701830

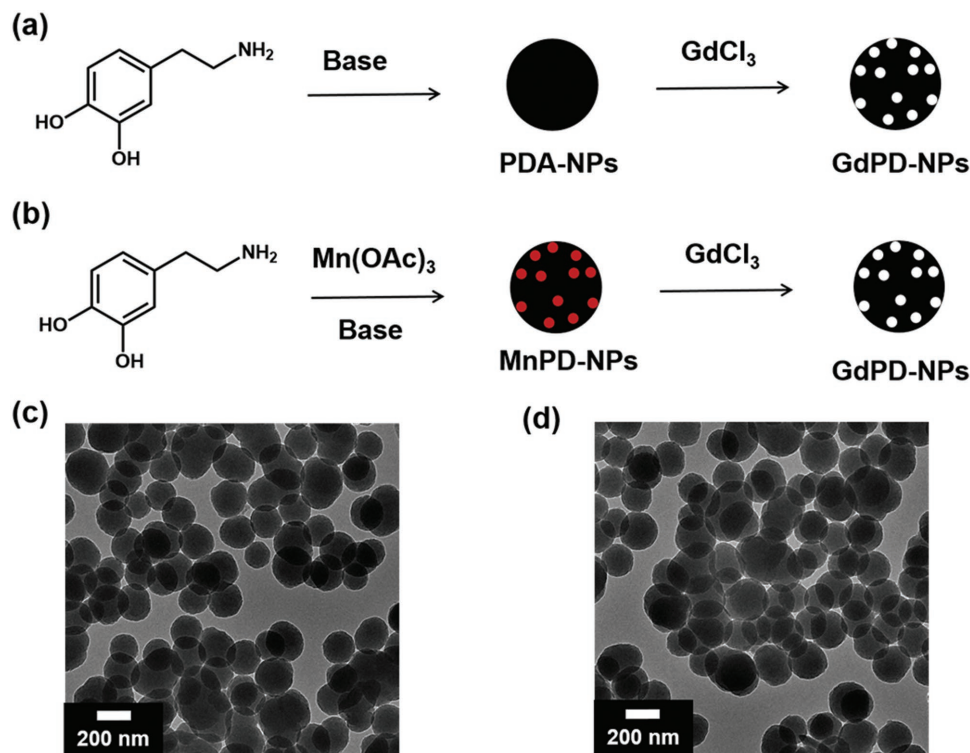


Figure 1. Preparation of GdPD-NPs (Gd-*i* (*i* = 1–5)): a) Postparticle formation doping strategy used to generate **Gd-1**. b) The prepolymerization doping strategy used to generate particles **Gd-2**, **Gd-3**, **Gd-4**, and **Gd-5**. White and red dots represent Gd(III) and Mn(III) ions, respectively. c) TEM micrograph of Mn(III)-doped PD-NPs (**Mn-4**) and d) corresponding GdPD-NPs (**Gd-4**). Gd loadings for **Gd-1**, **Gd-2**, **Gd-3**, **Gd-4**, and **Gd-5** are 2%, 3%, 5%, 11%, and 17%, respectively.

often results in r_1 values that are lower than theory would suggest based on the tumbling rates of the macromolecule or particle. The major limiting factors in many of these formulations have been the relatively slow rate of exchange of the bound water ($k_{ex} = 1/\tau_M$) and the occurrence of fast, local rotational motion of the Gd(III)-complex about the linker that connects it to the nanoparticle.^[5]

The strong metal binding ability of catechol-based functional groups has led to an interest in polydopamine (PD)-based nanoparticles (PD-NPs) in a growing number of research areas, including bioimaging,^[7] battery materials,^[8] catalysis,^[9] and environmental remediation.^[10] In addition, PD-NPs and naturally occurring melanin-based nanoparticles doped with Fe(III) and Mn(II) have been reported as MRI contrast agents.^[11] Recently, a prepolymerization doping strategy was reported to prepare Fe(III)-loaded PD-NPs in a single pot.^[12] However, adapting this procedure to synthesize high and tunable Gd(III)-content PD-NPs has remained a challenge.^[13] In addition, previous strategies do not result in ultrahigh relaxivity, and we expect to generate high relaxivity close to the theoretic limit.^[13c] Unlike transition metals such as Zn(II), Fe(III), and Mn(III), the methodology of introducing metal salts during the polymerization of dopamine is not compatible for the incorporation of the Gd(III) ion. Therefore, we developed a metal displacement method for the synthesis of a series of Gd(III)-polydopamine nanoparticles (GdPD-NPs) with variable Gd loadings, allowing an investigation of the basic properties of these materials in the context of their MRI contrast agents' performance. Given

the high coordination number of Gd(III)-complexes, fast H₂O exchange, weak antiferromagnetic superexchange interactions, and strong anchoring chelation provided by the PDA catechol moiety, we expect to generate high relaxivity close to the theoretic limit.

We first prepared GdPD-NPs using a postparticle formation doping strategy (**Figure 1**). PD-NPs were synthesized via auto-oxidation and polymerization of dopamine under basic conditions.^[14] The resulting nanoparticles were characterized by transmission electron microscopy (TEM) and dynamic light scattering (DLS) to quantify size and uniformity (Figures S1 and S2, Supporting Information). TEM shows spherical particles with diameters of ≈ 160 nm. After complexation with Gd, the morphology remains unchanged (Figure S1, Supporting Information). This is consistent with previous studies on iron-loaded polydopamine nanoparticles (FePD-NPs). Inductively coupled plasma atomic emission spectroscopy (ICP-OES) analysis was used to determine the Gd loadings to be 2 wt% ($\text{mass}_{\text{Gd}}/\text{mass}_{\text{GdPD-NP}}$). Though this postparticle formation doping strategy was successfully applied to prepare GdPD-NPs, the approach is limited to low Gd loading. Regardless Gd(III) could not be incorporated via the prepolymerization doping route as described in previous sections. This route does not produce uniform nanoparticles (Figure S3, Supporting Information). Additionally, the resulting nanoaggregates are colloidally unstable after polymerization and thus unsuitable for the analysis of their MRI performance. Therefore, we devised a strategy to first synthesize MnPD-NPs with controllable

Table 1. Selected relaxation parameters obtained from the analysis of NMRD profiles (298 K).

Gd- ⁱ) ^{a)}	r_1 [mM ⁻¹ s ⁻¹] ^{b)}	Δ^2 [10 ¹⁸ s ⁻²] ^{c)}	τ_V [ps] ^{c)}	τ_R [ns]	r [Å] ^{d)}	q	τ_M [ns] ^{d)}
Gd-1	63.4	8.1 ^{d)}	17 ^{d)}	1.5 ± 0.2	3.0	1.8 ± 0.1	30
Gd-2	56.9	8.1 ^{d)}	17 ^{d)}	1.4 ± 0.1	3.0	1.6 ± 0.1	30
Gd-3	74.6	8.4 ± 1.1	16 ± 1	1.5 ± 0.3	3.0	2 ^{d)}	30
Gd-4	52.3	8.1 ^{d)}	17 ^{d)}	1.4 ± 0.1	3.0	1.4 ± 0.1	30
Gd-5	35.1	8.1 ± 0.9	17 ± 1	1.2 ± 0.3	3.0	1 ^{d)}	30

^{a)}The outer-sphere component of the relaxivity was estimated using standard values for the distance of closest approach a (4 Å) and the relative diffusion coefficient of solute and solvent D (2.2×10^{-5} cm² s⁻¹); ^{b)}60 MHz; ^{c)}The parameters for electronic relaxation are used as empirical fitting parameters and do not have a real physical meaning for slowly tumbling nanosized systems. Low-field data, those most affected by electronic relaxation, were not included in data analysis; ^{d)}Fixed during the fit.

Mn(III) loadings. These structures served as templates with Mn(III) binding sites primed for displacement when treated with GdCl₃. MnPD-NPs were prepared through the oxidative polymerization of dopamine in the presence of Mn(III) salts under basic conditions as previously reported.^[15a] We initially observe a red solution suggesting the formation of an Mn(III)-catecholate species,^[15b] which is polymerized to form black MnPD-NPs. The incorporation of Mn can be confirmed by X-ray photoelectron spectroscopy (XPS). As shown in Figure S4 (Supporting Information), the XPS spectrum of MnPD-NPs showed a typical binding energy (641.7 eV) at the characteristic peak of Mn(2p_{3/2}), which can be assigned to Mn(III). Recent magnetometry studies on materials prepared via this method for MnPD-NPs have corroborated the trivalent oxidation state, likely due to the highly oxidative conditions of the polymerization.^[15a]

After work-up and isolation of the MnPD-NPs, a simple ion exchange procedure was attempted. MnPD-NPs were suspended in an aqueous solution of excess GdCl₃ and incubated for ≈12 h. The extent of the displacement reaction was determined by the analysis of XPS and ICP-OES data before and after the Gd(III) incubation. As shown in Figure S4 (Supporting Information), the initial survey scan spectrum of MnPD-NPs exhibits binding energies at the characteristic peaks of C(1s), O(1s), N(1s), and Mn(2p), thus confirming their presence in the original MnPD-NPs. After the displacement reaction, the survey scan spectrum exhibits the characteristic peaks of C(1s), O(1s), N(1s), and Gd(4d), and the characteristic peaks of Mn2p have been eliminated. The resulting nanoparticles show a Gd loading of 11 wt% and a negligible amount of Mn (0.006 wt%) by ICP-OES measurement, consistent with the XPS data. Therefore, we hypothesize that the Mn(III) was replaced by Gd(III) due to weaker binding of Mn(III) to polydopamine compared with Gd(III).^[15c] These GdPD-NPs were characterized by TEM and DLS with no change in morphology compared to the initial MnPD-NP species (Figure 1d and Figures S1 and S2 and Table S1, Supporting Information). In addition, by choosing templates with increased amounts of Mn(III), we can achieve higher Gd loadings of up to 17 wt% (Table S1, Supporting Information). We also measure zeta potential of all five samples. All of these samples exhibited highly negative zeta potential value (Gd-1: -17.8 V; Gd-2: -31.3 V; Gd-3: -50.6 V; Gd-4: -20.7 V; Gd-5: -24.7 V), suggesting the high stability of these systems in aqueous solution.

In our previous study describing tunable Fe(III) loadings in PD-NPs via the prepolymerization chelation strategy, we found that antiferromagnetic coupling between Fe(III) centers lowered their r_1 as we increased Fe(III) loadings in the particles.^[12] We hypothesized that Gd(III) would exhibit much less antiferromagnetic coupling because of the poor radial extension of the f-orbitals. This implies that increasing the Gd(III) loading would not lead to the r_1 losses observed for Fe(III), but rather a dramatic increase in per-particle relaxivity, with the only potential for diminishing returns being core-localized metal ions having less access to water. Therefore, we aimed to determine optimal loading conditions by measuring r_1 as a function of Gd(III) loading.

The measurement of r_1 and transverse water proton relaxation rates (r_2) as a function of applied magnetic field for the five GdPD-NPs (Table 1) was undertaken to assess their T_1 contrast enhancing ability. Nuclear magnetic relaxation dispersion (NMRD) allows accurate determination of the field dependence of r_1 that arises from magnetic interactions between the metal centers and the solvent (Figure 2).^[3b,16] The NMRD profiles are characteristic of slowly rotating systems with a shallow decrease of r_1 at about 1–5 MHz and a broad and pronounced peak centered at 30–50 MHz. All five curves share similar characteristics across the entire frequency range, but appear offset from one

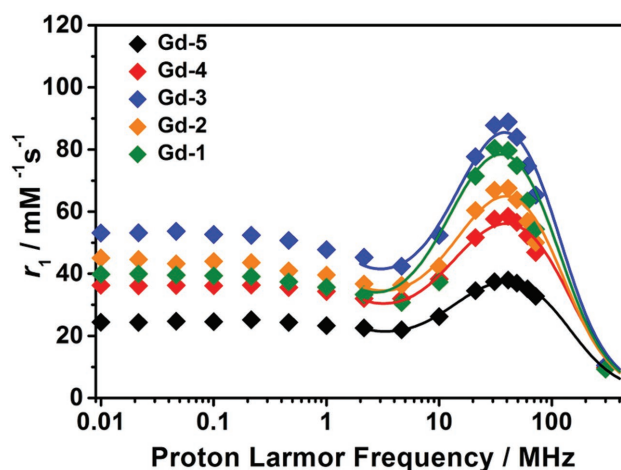


Figure 2. ¹H NMRD profiles for Gd-*i* (*i* = 1–5). The x-axis is proton Larmor frequency and the y-axis is r_1 value per Gd(III) ion for each sample.

another by a scaling factor. The fact that the NMRD profiles exhibit a common shape but offset in this way suggests that the origin of the relaxivity differences must be a parameter that directly influences r_1 without being field-dependent. Relaxivity scales either with the hydration number q or with the distance, r_{GdH} , between the coordinated water proton and the Gd(III) $S = 7/2$ electron spin. According to data for small Gd(III) chelates, the r_{GdH} values are typically found in the narrow range of $\approx 3.0\text{--}3.2$ Å, with no evidence of a dependence on the coordination geometry of the metal complex.^[17] Therefore, it is plausible that the different amplitude of the five NMRD profiles reflects a change in the hydration state of the Gd(III) ions. Therefore, we first analyzed **Gd-5** assuming the presence of one water molecule in the inner coordination sphere of Gd(III) centers throughout the structure, as the relaxivity values are in line with those of other macromolecular Gd-based systems with $q = 1$.^[2a,5,18] We note that only frequencies above 3 MHz were analyzed, as Solomon–Bloembergen–Morgan theory is not adequate to account for the data at low magnetic fields in the case of slowly rotating systems. The temperature dependency of r_1 at high field clearly indicates the occurrence of fast exchange conditions. That is, r_1 is not limited by water exchange. We then fixed this parameter at 30 ns and performed the fit treating three parameters as variables, namely, the overall rotational correlation time (τ_R), the correlation time for the transient zero-field splitting (ZFS; τ_V), and the amplitude of the transient ZFS (Δ^2). The best-fit parameters obtained for the GdPD-NPs from the analysis of ^1H NMRD data are shown in Table 1. We conclude that the tight packing of Gd-centers at catechol groups throughout crosslinked polymers within the NPs results in a rotationally restricted system at the metal centers and their chelates. The absence of internal rotation of the Gd-chelates leads to a very good fit, even at high frequencies, with a single global rotational correlation time of 1.2 ns. Likewise, the NMRD profile of **Gd-3** can be fitted by simply assuming $q = 2$. The other parameters vary only marginally reinforcing the hypothesis that relaxivity changes are associated with changes in the state of hydration of the paramagnetic centers. A q value of 2 could be associated with a larger number of Gd ions exposed to the surface and more accessible to water molecules, whereas $q = 1$ might arise as an average between the Gd centers on the surface ($q = 2$) and those in the inner core of the NPs, not accessible to water ($q = 0$). The NMRD profiles of NPs **Gd-4**, **Gd-2**, and **Gd-1** were analyzed by fitting only q and τ_R . The best results were obtained with the parameters shown in Table 1, where the rotational correlation time is essentially unchanged and the effective q value scales with the relaxivity, from 1.4 to 1.8.

The r_1 values (1.4 T; 60 MHz) demonstrate the presence of facile relaxation in all five samples (Table S2, Supporting Information). **Gd-3** has an r_1 value of $75 \text{ mM}^{-1} \text{ s}^{-1}$, 20-fold higher than commercially used Gd-based contrast agents (i.e., Gd-DOTA) and superior to many previously reported macromolecules and nanoscale formulations (such as liposomes and dendritic species).^[19] It is also the highest one among the five tested samples. Therefore 5% is the optimal loading conditions for achieving the highest per Gd ion relaxivity, which is approaching the theoretical limit. When increasing the Gd loading to 17% (**Gd-5**), the r_1 value remains relatively high ($35 \text{ mM}^{-1} \text{ s}^{-1}$). The decrease of r_1 may be due

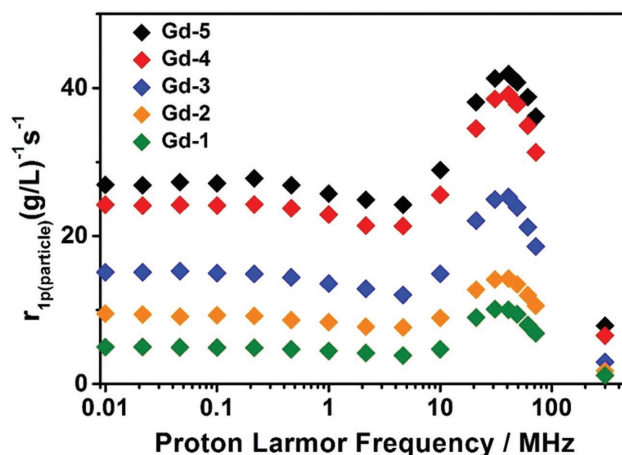


Figure 3. ^1H NMRD profiles for Gd- i ($i = 1\text{--}5$). The x-axis is proton Larmor frequency and the y-axis is r_1 value per nanoparticle for each sample.

to the larger size of **Gd-5** preventing water coordination of paramagnetic centers within the core of the particle. The r_2/r_1 ratios at various field strengths (20–70 MHz) were determined (Figure S5, Supporting Information) and not surprisingly, these ratios increase with increasing proton Larmor frequency, with the highest value being under 3, indicating that **Gd-1–5** act as T_1 -weighted contrast agents with relatively little interference from T_2 darkening.

Given that each particle contains many chelated Gd(III) ions, it is interesting to consider the “per-particle relaxivity” ($r_{1\text{p}(\text{particle})}$) to describe the local concentration necessary to achieve the desirable T_1 MRI contrast under different magnetic fields (Figure 3).^[20] Interestingly, plots of $r_{1\text{p}(\text{particle})}$ and $r_{1\text{p}(\text{Gd(III)})}$ show different trends. Whereas $r_{1\text{p}(\text{Gd(III)})}$ reveals a maximum relaxivity for **Gd-3**, the plot of $r_{1\text{p}(\text{particle})}$ shows that relaxivity increases monotonically with doping amount on a per-particle basis. Thus, **Gd-5** exhibits the highest per-particle relaxivity, about five times larger than the **Gd-1** at 60 MHz (Figure 3). These data lead to the intuitive result that highly paramagnetically doped particles are superior to those doped with lower levels of Gd(III) ions.

To evaluate the potential utility of GdPD-NPs as T_1 -weighted contrast agents at high magnetic fields, we calculated their r_1 values and captured T_1 -weighted MR images using a volume coil with a 7-tesla (T) MRI scanner. The T_1 relaxation times became shorter and the phantom image became brighter as the Gd(III) concentrations increased (Figure 4a–d), suggesting that the GdPD-NPs accelerated the recovery of net magnetization. At 7 T, **Gd-3** has the highest r_1 value ($r_1 = 10.5 \text{ mM}^{-1} \text{ s}^{-1}$), while the other four samples exhibit only slightly lower values. This value is roughly four times higher than common commercial contrast agents such as Gd-DOTA ($r_1 = 3.0 \text{ mM}^{-1} \text{ s}^{-1}$) and Gd-DTPA ($r_1 = 3.1 \text{ mM}^{-1} \text{ s}^{-1}$).^[21] Additionally, the rough equivalence of **Gd-1–5** r_1 values means that a significantly lower Gd(III) ion dosage can be used without sacrificing the contrast enhancement ability. The r_2/r_1 values (Table S3, Supporting Information) are larger compared with the ones at 1.4 T due to the enhanced T_2 effect at high field. To demonstrate the potential for **Gd- i** to be used as contrast agents, they were incubated with HeLa cells and shown to provide enhanced positive con-

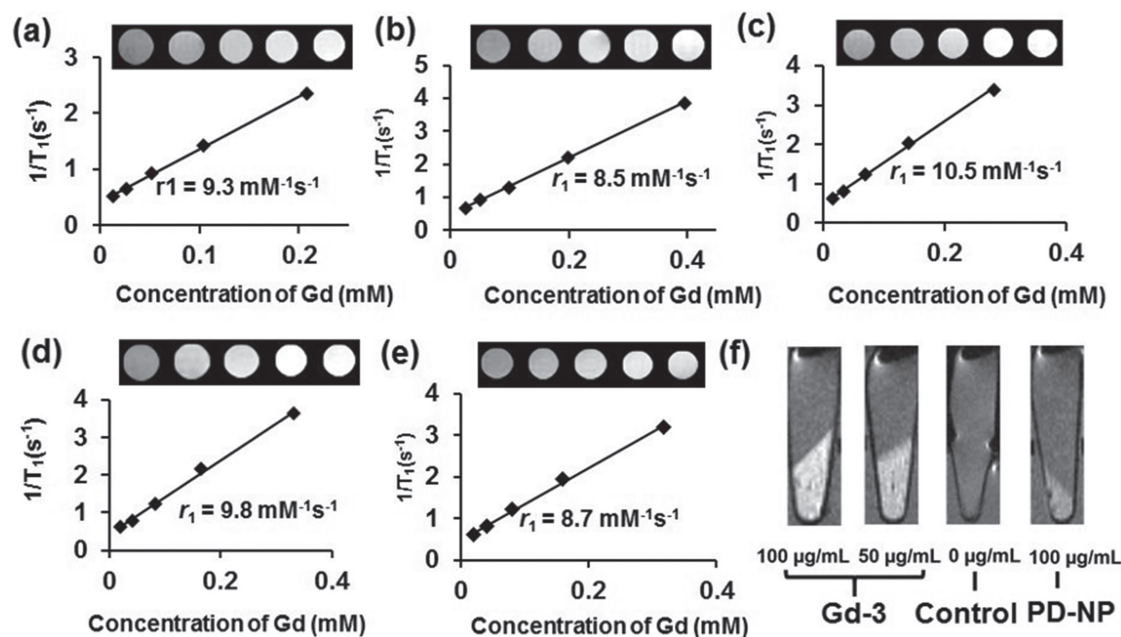


Figure 4. MRI characterization of Gd-*i* (*i* = 1–5) on a Bruker 7-T magnet. Plots of $1/T_1$ versus Gd(III) concentration and its corresponding image of a) Gd-1, b) Gd-2, c) Gd-3, d) Gd-4, and e) Gd-5. f) In vitro T_1 -weighted MR images of HeLa cells incubated with Gd-3 and PD-NP at different concentrations for 24 h.

trast in T_1 -weighted MR images as compared to control cells (Figure 4). Overall, the high T_1 relaxivity and low r_2/r_1 ratio of GdPD-NPs could make them suitable as low dosage, Gd-based contrast agents for T_1 -weighted MRI measurements.

A key prerequisite for in vivo imaging applications is low toxicity. For Gd-*i* to be useful, Gd(III) ions must not be susceptible to transmetallation as this would result in a release of potentially harmful free Gd(III) ions.^[22] Thus it is important to examine the selectivity of these nanoparticles for Gd(III) over physiological metal ions, such as Ca(II) and Zn(II). We use Gd-3 to examine stability of Gd(III) coordination over Ca(II) and Zn(II) at their maximum human blood concentration ($2.5 \times 10^{-3} \text{ M}$ for Ca(II) and $0.15 \times 10^{-3} \text{ M}$ for Zn(II)). Gd-3 was incubated with aqueous CaCl₂ and ZnCl₂ solutions for 7 d, followed by multiple washing and centrifugation steps to remove free metal ions. The sample was then analyzed via ICP-OES to show no significant release of Gd(III) ion on this timescale (Figure S6, Supporting Information). The stability of Gd-3 in various media was also examined. We observe that the amount of chelated Gd(III) ion does not change significantly over time in water, 4-(2-hydroxyethyl)-1-piperazineethanesulfonic acid (HEPES) and Phosphate Buffered Saline (PBS) buffer (Figure S7, Supporting Information). Although the cell viability of PD-NPs had already been confirmed,^[23] the cytotoxicity of GdPD-NPs has not yet been evaluated. Nanoparticles with negatively charged surfaces often exhibit a lower cytotoxicity compared to those with positively charged ones.^[24] We tested the toxicity of samples with various loadings of Gd(III) (Gd-1, Gd-3, Gd-4, Gd-5, and PD-NP). The results showed no obvious cytotoxicity after incubation with Gd-1, Gd-3, or Gd-4 at levels up to $125 \mu\text{g mL}^{-1}$ within 48, while the Gd-5 sample showed some cytotoxicity at high concentration ($125 \mu\text{g mL}^{-1}$) that may come from the high content of Gd(III) inside the nanoparticle

(Figure S8, Supporting Information). We recently found that polydopamine nanoparticles undergo a similar degradation pathway as natural melanosomes.^[25] In addition, Gd(III) is also known to have high affinity to catechol units.^[26] Therefore we anticipate that the GdPD-NPs, upon possible degradation in vivo over the long term, would stay in chelated form.

In our previous work,^[12] it was shown that increasing Fe(III) ion concentration within polydopamine nanoparticles led to antiferromagnetic coupling that correlated with decreases in MR contrast. To investigate whether Gd(III)–Gd(III) coupling or the formation of Gd oxide phases at high concentrations could be playing a role in the decrease in r_1 , the magnetic properties of GdPD-NPs were investigated by variable-temperature magnetic susceptibility measurements from 2 to 300 K under a 5000 Oe magnetic field (Figure S9, Supporting Information). Unlike in FePD-NPs, there is no appreciable deviation from single-ion, spin-only behavior ($\chi_M T = 7.88 \text{ emu K cm}^{-3} \text{ mol}^{-1}$) for the three GdPD-NP samples that were tested. This indicates a nearly complete lack of antiferromagnetic coupling between Gd(III) centers in the polydopamine systems. These data indicate that the drop in per-Gd(III) relaxivity at high concentrations must be dependent on the lack of solvent access to core ions in the larger particles. In addition, the magnetic susceptibility of the $S = 2$ Mn(III) ion is much smaller than that of the $S = 7/2$ Gd(III) ion ($\chi_M T_{\text{Mn(III)}}, 300 \text{ K} = 3 \text{ emu K mol}^{-1} < \chi_M T_{\text{Gd(III)}}, 300 \text{ K} = 7.88 \text{ emu K mol}^{-1}$). Even if some small amount of Mn(III) ions remains chelated, their contribution to the magnetic susceptibility can be considered negligible.

In conclusion, we report a simple and scalable synthetic method of generating GdPD-NPs. We describe Gd PD-NPs as contrast agents with several potential advantages: (1) the nanoscale formulation and crosslinked nature of the Gd-chelates leads to slow molecular tumbling increasing contrast;

(2) restriction of the free rotation of the chelates extends to the surface bound Gd, due to the crosslinked polydopamine 3D network; (3) the catechols in the 3D crosslinked network are strained, leading to the formation of unsaturated Gd-catecholate, allowing high hydration states ($q > 1$). Finally, these factors result in our observation that the as-prepared nanoparticles show significant MRI signal enhancement and the value of longitudinal relaxivity is as high as $75 \text{ mM}^{-1} \text{ s}^{-1}$ at 1.4 T and $10.5 \text{ mM}^{-1} \text{ s}^{-1}$ at 7 T for **Gd-3**. While the relatively large particle size ($>100 \text{ nm}$) limits the use in targeting to the interstitial space of tissues,^[27] these nanoparticles may have potential applications in tumor imaging due to the enhanced permeability and retention effect.^[11b,13b,28]

Supporting Information

Supporting Information is available from the Wiley Online Library or from the author.

Acknowledgements

The authors thank the AFOSR for generous funding through a PECASE to N.C.G. (FA9550-11-1-0105). M.B. acknowledges support of the "Compagnia di San Paolo" (CSP-2012 NANOPROGLY Project). Y.L. acknowledges financial support from the State Key Laboratory of Polymer Materials Engineering, Sichuan University (Grant No. sklprme2016-3-03). This work made use of the Keck-II facility of Northwestern University's NUANCE Center, which has received support from the Soft and Hybrid Nanotechnology Experimental (SHyNE) Resource (NSF ECCS-1542205); the MRSEC program (NSF DMR-1121262) at the Materials Research Center; the International Institute for Nanotechnology (IIN); the Keck Foundation; and the State of Illinois, through the IIN. Dr. S.H. acknowledges the support from FISP award (C6007) and Air Force Office of Scientific Research (AFOSR) FA9550-15-1-0273.

Conflict of Interest

The authors declare no conflict of interest.

Keywords

antiferromagnetic coupling, contrast agent, magnetometry, MRI, polydopamine

Received: May 31, 2017

Revised: August 4, 2017

Published online: October 10, 2017

- [1] J. Enders, E. Zimmermann, M. Rief, P. Martus, R. Klingebiel, P. Asbach, C. Klessen, G. Diederichs, T. Bengner, U. Teichgräber, B. Hamm, M. Dewey, *BMC Med. Imaging* **2011**, *11*, 4.
[2] a) P. Caravan, J. J. Ellison, T. J. McMurry, R. B. Lauffer, *Chem. Rev.* **1999**, *99*, 2293; b) L. M. Randolph, C. L. M. LeGuyader, M. E. Hahn, C. M. Andolina, J. P. Patterson, R. F. Mattrey, J. E. Millstone, M. Botta, M. Scadeng, N. C. Gianneschi, *Chem. Sci.* **2016**, *7*, 4230; c) Z. Zhou, Z.-R. Lu, *Wiley Interdiscip. Rev.: Nanomed. Nanotechnol.* **2013**, *5*, 1.

- [3] a) P. Caravan, *Chem. Soc. Rev.* **2006**, *35*, 512; b) S. Aime, M. Botta, E. Terreno, *Adv. Inorg. Chem.* **2005**, *57*, 173; c) Z. Wang, Y. Li, Y. Huang, M. P. Thompson, C. L. M. LeGuyader, S. Sahu, N. C. Gianneschi, *Chem. Commun.* **2015**, *51*, 17108; d) K. R. Maravilla, J. A. Maldjian, I. M. Schmalfluss, M. J. Kuhn, B. C. Bowen, F. J. Wippold, V. M. Runge, M. V. Knopp, S. Kremer, L. J. Wolansky, N. Anzalone, M. Essig, L. Gustafsson, *Radiology* **2006**, *240*, 389; e) S. He, N. J. J. Johnson, V. A. Nguyen Huu, E. Cory, Y. Huang, R. L. Sah, J. V. Jokerst, A. Almutairi, *Nano Lett.* **2017**, *17*, 4873.
[4] a) A. J. L. Villaraza, A. Bumb, M. W. Brechbiel, *Chem. Rev.* **2010**, *110*, 2921; b) N. J. J. Johnson, S. He, V. A. Nguyen Huu, A. Almutairi, *ACS Nano* **2016**, *10*, 8299.
[5] M. Botta, L. Tei, *Eur. J. Inorg. Chem.* **2012**, *2012*, 1945.
[6] J. J. Yang, J. Yang, L. Wei, O. Zurkiya, W. Yang, S. Li, J. Zou, Y. Zhou, A. L. W. Maniccia, H. Mao, F. Zhao, R. Malchow, S. Zhao, J. Johnson, X. Hu, E. Krogstad, Z.-R. Liu, *J. Am. Chem. Soc.* **2008**, *130*, 9260.
[7] a) X. Zhang, S. Wang, L. Xu, L. Feng, Y. Ji, L. Tao, S. Li, Y. Wei, *Nanoscale* **2012**, *4*, 5581; b) Y. Li, Y. Huang, Z. Wang, F. Carniato, Y. Xie, J. P. Patterson, M. P. Thompson, C. M. Andolina, T. B. Ditri, J. E. Millstone, J. S. Figueroa, J. D. Rinehart, M. Scadeng, M. Botta, N. C. Gianneschi, *Small* **2016**, *12*, 668; c) Q. Fan, K. Cheng, X. Hu, X. Ma, R. Zhang, M. Yang, X. Lu, L. Xing, W. Huang, S. S. Gambhir, Z. Cheng, *J. Am. Chem. Soc.* **2014**, *136*, 15185.
[8] a) H. Jiang, L. Yang, C. Li, C. Yan, P. S. Lee, J. Ma, *Energy Environ. Sci.* **2011**, *4*, 1813; b) H. Jiang, T. Sun, C. Li, J. Ma, *RSC Adv.* **2011**, *1*, 954.
[9] K. Ai, Y. Liu, C. Ruan, L. Lu, G. M. Lu, *Adv. Mater.* **2013**, *25*, 998.
[10] J. Fu, Z. Chen, M. Wang, S. Liu, J. Zhang, J. Zhang, R. Han, Q. Xu, *Chem. Eng. J.* **2015**, *259*, 53.
[11] a) K.-Y. Ju, J. W. Lee, G. H. Im, S. Lee, J. Pyo, S. B. Park, J. H. Lee, J.-K. Lee, *Biomacromolecules* **2013**, *14*, 3491; b) Z.-H. Miao, H. Wang, H. Yang, Z.-L. Li, L. Zhen, C.-Y. Xu, *ACS Appl. Mater. Interfaces* **2015**, *7*, 16946.
[12] Y. Li, Y. Xie, Z. Wang, N. Zang, F. Carniato, Y. Huang, C. M. Andolina, L. R. Parent, T. B. Ditri, E. D. Walter, M. Botta, J. D. Rinehart, N. C. Gianneschi, *ACS Nano* **2016**, *10*, 10186.
[13] a) W.-W. Cai, L.-J. Wang, S.-J. Li, X.-P. Zhang, T.-T. Li, Y.-H. Wang, X. Yang, J. Xie, J.-D. Li, S.-J. Liu, W. Xu, S. He, Z. Cheng, Q.-L. Fan, R.-P. Zhang, *J. Biomed. Mater. Res. A* **2017**, *105*, 131; b) S. Cho, W. Park, D.-H. Kim, *ACS Appl. Mater. Interfaces* **2017**, *9*, 101; c) P. Caravan, C. T. Farrar, L. Frullano, R. Uppal, *Contrast Media Mol. Imaging* **2009**, *4*, 89.
[14] Y. Liu, K. Ai, J. Liu, M. Deng, Y. He, L. Lu, *Adv. Mater.* **2013**, *25*, 1353.
[15] a) Z. Wang, Y. Xie, Y. Li, Y. Huang, L. R. Parent, T. B. Ditri, N. Zang, J. D. Rinehart, N. C. Gianneschi, *Chem. Mater.* **2017**, <https://doi.org/10.1021/acs.chemmater.7b02262>; b) M. J. Sever, J. J. Wilker, *Dalton Trans.* **2004**, *0*, 1061; c) B. Larsson, H. Tjälve, *Acta Physiol.* **1978**, *104*, 479.
[16] S. H. Koenig, R. D. Brown, *Prog. Nucl. Magn. Reson. Spectrosc.* **1990**, *22*, 487.
[17] P. Caravan, A. V. Astashkin, A. M. Raitsimring, *Inorg. Chem.* **2003**, *42*, 3972.
[18] A. Accardo, D. Tesaro, L. Aloj, C. Pedone, G. Morelli, *Coord. Chem. Rev.* **2009**, *253*, 2193.
[19] J. Tang, Y. Sheng, H. Hu, Y. Shen, *Prog. Polym. Sci.* **2013**, *38*, 462.
[20] G. Sitbon, S. Bouccara, M. Tasso, A. Francois, L. Bezdetsnaya, F. Marchal, M. Beaumont, T. Pons, *Nanoscale* **2014**, *6*, 9264.
[21] I. M. Noebauer-Huhmann, P. Szomolanyi, V. Juras, O. Kraff, M. E. Ladd, S. Trattig, *Invest. Radiol.* **2010**, *45*, 554.

- [22] a) P. H. Kuo, E. Kanal, A. K. Abu-Alfa, S. E. Cowper, *Radiology* **2007**, *242*, 647; b) J.-M. Idée, M. Port, I. Raynal, M. Schaefer, S. Le Greneur, C. Corot, *Fundam. Clin. Pharmacol.* **2006**, *20*, 563.
- [23] K.-Y. Ju, Y. Lee, S. Lee, S. B. Park, J.-K. Lee, *Biomacromolecules* **2011**, *12*, 625.
- [24] E. Fröhlich, *Int. J. Nanomed.* **2012**, *7*, 5577.
- [25] Y. Huang, Y. Li, Z. Hu, X. Yue, M. T. Proetto, Y. Jones, N. C. Gianneschi, *ACS Cent. Sci.* **2017**, *3*, 564.
- [26] G. E. Freeman, K. N. Raymond, *Inorg. Chem.* **1985**, *24*, 1410.
- [27] S. Barua, S. Mitragotri, *Nano Today* **2014**, *9*, 223.
- [28] R. Ge, M. Lin, X. Li, S. Liu, W. Wang, S. Li, X. Zhang, Y. Liu, L. Liu, F. Shi, H. Sun, H. Zhang, B. Yang, *ACS Appl. Mater. Interfaces* **2017**, *9*, 19706.